Two-Phase Flow Modeling with Discrete Particles*

Glen A. Mortensen
Idaho National Engineering Laboratory
EG&G Idaho, Inc.

EGG-M--92026

DE92 017850

John A. Trapp
University of Colorado - Denver
and
Idaho National Engineering Laboratory

March 23, 1992

For submission to the
Two-Phase Flow in Energy Exchange Systems Session
of the 1992 ASME Winter Annual Meeting
November 8-13, 1992
Anaheim, California

DRAFT

* Work supported by the U. S. Department of Energy, Assistant Secretary for Conservation and Renewable Energy, under DOE Field Office, Idaho, Contract DE-AC07-76ID01570.

ABSTRACT

The design of efficient heat exchangers in which the working fluid changes phase requires accurate modeling of two-phase fluid flow. The local Navier-Stokes equations form the basic continuum equations for this flow situation. However, the local instantaneous model using these equations is intractable for all but the simplest problems. All the practical models for two-phase flow analysis are based on equations that have been averaged over control volumes. These models average out the detailed description within the control volumes and rely on flow regime maps to determine the distribution of the two phases within a control volume. Flow regime maps depend on steady state models and probably are not correct for dynamic models.

Numerical simulations of the averaged two-phase flow models are usually performed using a two-fluid Eulerian description for the two phases. Eulerian descriptions have the advantage of having simple boundary conditions, but the disadvantage of introducing numerical diffusion, i.e., sharp interfaces are not maintained as the flow develops, but are diffused. Lagrangian descriptions have the advantage of being able to track sharp interfaces without diffusion, but they have the disadvantage of requiring more complicated boundary conditions.

This paper describes a numerical scheme and attendant computer program, DISCON2, for the calculation of two-phase flows that does not require the use of flow regime maps. This model is intermediate between the intractable local instantaneous and the averaged two-fluid model. This new model uses a combination of an Eulerian and a Lagrangian representation of the two phases. The dispersed particles (bubbles or drops) are modeled individually using a large representative number of particles, each with their own Lagrangian description. The continuous phases (liquid or gas) use an Eulerian description. Since the dispersed phase particles are modeled directly, the model avoids the numerical diffusion associated with Eulerian models.

Previous work along this line has been done by researchers at LANL using the KIVA computer program [Amsden, 1989] to model spray-combustion processes, and researchers at JAYCOR using the BUBBLE computer program [Stuhmiller, 1989] to model bubbly flow. The KIVA program models drops sprayed into a continuous gas, and the BUBBLE program models one continuous liquid phase and one discrete bubble phase. Our computer program, DISCON2, will eventually extend these models to two continuous phases (liquid and gas) each containing a discrete phase (bubbles and droplets). However, the present paper describes only the one-continuous phase, one-discrete phase model. It solves the Eulerian continuity, momentum, and energy equations for the liquid in each control volume, and the Lagrangian mass, momentum, and energy equations for each bubble. No explicit flow regime map is used in the model. Heat addition from the wall is modeled using a subcooled boiling model. DISCON2 has been used to simulate the boiling of liquid water in a flow channel with a constant wall heat flux, and the results of these calculations are presented.

NOMENCLATURE

a = acceleration

A = area

B = any combination of variables

C = coefficient

C_p = heat capacity

D_e = equivalent hydraulic diameter

f = interface or wall drag coefficient

F = force particle exerts on continuous phase

g = acceleration of gravity

G = mass flow rate

h = film heat transfer coefficient

i = enthalpy

M = multiplier

Nu Nusslet Number

P = pressure

Pe : Pecklet Number

Q = energy

r = radius

Re : Reynolds Number

St = Stanton Number

t = time

T = temperature

u = velocity

V = volume

w = temperature weighting factor

x = distance

α = volume fraction

Δ = increment

ε = entropy

Γ = mass transfer rate

θ = interface temperature

ρ = density

Subscripts

a = added mass

b = bubble

d = drag

f = frontal

g = gas

i = particle index

j = momentum cell index

k = continuity cell index

l = liquid

sat = saturation

w = wall or wake

Superscripts

n = time level

1. INTRODUCTION

The modeling and numerical simulation of two-phase flow continues to pose complex and challenging problems. Descriptions based on the local instantaneous Navier-Stokes equations with internal interfaces are clearly intractable in all but the simplest cases. The present state-of-the-art model in two-phase flow is based upon the averaged two-fluid concept. This paper describes a model based on a multiphase description that is intermediate between the numerically intractable local instant description and the fully averaged two-fluid model. In particular, the dispersed phases are modeled using Lagrangian descriptions that are embedded within the Eulerian description for the continuous phases. This approach: (1) permits the statistical features of the dispersed phases to be modeled directly, (2) permits the prediction of flow regime transitions, and (3) avoids the numerical diffusion associated with Eulerian implementations of multi-field descriptions. Similar models have previously been successfully used to model fuel sprays [Dukowicz, 1979, O'Rourke, 1981, O'Rourke, 1987, and Amsden, 1989]. Their extension to two-phase flow presents additional challenges related to void fraction coupling between phases and particles that are no longer small compared to computational cell sizes.

A computer code, DISCON2, has been written to implement this model. The basic concept of the model is to describe the motion of the dispersed phases using Lagrangian descriptions. The main motivation is to be able to predict flow regime transitions and represent a spectra of drop and bubble sizes. However, in order for the continuous and discrete phases to interact, it is necessary to relate the two descriptions. This interaction takes place through three mechanisms:

1. Phase coupling, because each phase occupies a volume not available to the other phase (void fraction coupling)
2. Interface drag between the phases (momentum coupling)
3. Interface energy and mass transfer (energy coupling)

The first mechanism proved the most difficult to implement numerically.

Shown at the left is the top section of a typical subcooled boiling DISCON2 simulation. As is evident in the graphic, spherical bubbles, elliptical bubbles, spherical cap bubbles, and slugs are generated as the simulation progresses.

Section 2 describes the discrete phase Lagrangian model equations, Section 3 describes the continuous phase Eulerian model equations, Section 4 describes the phase coupling models, Section 5 describes some additional models, Section 6 contains a summary of the basic equations, and Section 7 describes the solution scheme, Section 8 describes test problem calculations that have been performed, and Section 9 contains some conclusions. The references are in Section 10.

2. DISCRETE PHASE LAGRANGIAN MODEL EQUATIONS

The mass, momentum, and energy equations for each discrete particle, bubble in this case, are based on the average properties of that bubble. Because each bubble has its own position in space and is individually tracked, the conservation equations are ordinary differential equations governing the time evolution of mass, momentum, and energy. Each evolution equation includes appropriate interaction terms with the continuous phase, liquid in this case, through which the bubble is moving.

2.1. Discrete Phase Mass Equation

The conservation equations are written in a partially discretized form showing the time levels of all source terms. Any undifferentiated term without a time level shown is evaluated at the old, n^{th}, time level. All terms that are evaluated at the new time level contain an n+1 superscript. In the following, $\frac{dB}{dt}$ is understood to mean $\frac{B^{n+1} - B^n}{\Delta t}$, B stands for any variable or combination of variables.

The mass conservation equation for bubble t is,

$$\frac{d(\rho_{tb} V_{tb})}{dt} = -\Gamma_{tbl}^{n+1} \tag{1}$$

where Γ_{tbl} is the mass transfer rate from the bubble to the liquid phase. In the numerical implementation of all the discrete particle equations, the time derivatives of products are expanded into products of derivatives, and first-order forward differences are used with the coefficients evaluated at the old time level. Because the description of each particle is Lagrangian, the particle density and volume are functions of time only.

2.2. Discrete Phase Momentum Equation

The momentum balance for bubble t is,

$$\rho_{tb} V_{tb} \frac{du_{tb}}{dt} = \rho_{tb} V_{tb} g - F_{tb} \tag{2}$$

where F_{tb} is the force that the particle exerts on the continuous phase. This force is the sum of (i) the interphase drag force, (ii) the added mass force, and (iii) the interface force due to the mean pressure gradient about the particle.

$$F_{ib} = f_{ibl}\left[u_{ib}^{n+1} - \{\bar{u}_l\}_{ibl}\right] + C_{al}\{\bar{\rho}_l\}_{ib} V_{ib}\left(\frac{du_{ib}}{dt} - \{\bar{a}_l\}_{ib}\right) + V_{ib}\left[\frac{\partial P}{\partial x}\right]_{ib} \quad (3)$$

where

$$f_{ibl} = \left[0.5\{\bar{\rho}_l\}_{ib} C_{dib} A_{fib} |u_{ib} - \bar{u}_{ib}|\right] \quad (4)$$

is the interface drag coefficient, and the overbar signifies an average quantity. The bubble velocity is evaluated implicitly in the interface drag term, which removes the need for a small time step due to the large values of the interface drag coefficient, f_{ibl}.

2.3. Discrete Phase Energy Equation

The energy balance for bubble i is given by the following equation, which is written in terms of entropy, ε_i:

$$\frac{d(\rho_{ib}\varepsilon_{ib}V_{ib})}{dt} = -\varepsilon_{ib}\Gamma_{ibl}^{n+1} + \frac{h_{ib}A_{ibl}\left(\theta_{ibl}^{n+1} - T_{ib}^{n+1}\right)}{\theta_{ibl}} \quad (5)$$

The interface temperature is set to the saturation temperature at the location of the bubble.

The first term on the right-hand-side is the entropy transfer rate associated with the bubble–liquid mass transfer rate from inside the bubble to bubble-liquid interface surrounding the bubble. The second term is the entropy transfer rate associated with the heat transfer from the bubble-liquid interface surrounding the bubble to the inside of the bubble. The driving temperature difference for this heat transfer is the bubble-liquid interface temperature minus the internal bubble temperature. Since this last term is an entropy addition rate, it is divided by the temperature of the bubble-liquid interface.

2.4. Discrete Phase Kinetic Position Equation

A final equation to advance the bubble position, x_{ib}, is needed in this Lagrangian description. It is,

$$\frac{dx_{ib}}{dt} = u_{ib}^{n+1} \quad (6)$$

Modifications of equation (6) to include simple turbulence effects are described later. These modifications incorporate the fact that the bubbles are three-dimensional, and therefore, we use two additional kinematic position equations to track the bubble in the other two dimensions. However, our model does not include any interaction terms between the continuous phase and the discrete phase in these two perpendicular directions. We also use the three-dimensionality of the bubble in the coalescence model to compute the overlap between two bubbles to determine if they should be merged.

Equations (1) – (6) are solved for each bubble. Simulations with up to 10,000 bubbles have been made with the DISCON2 code.

3. CONTINUOUS PHASE EULERIAN MODEL EQUATIONS

The continuous phase equations are discretized using a staggered Eulerian mesh, shown in Fig. 1. Mass is conserved in each continuity cell, and momentum is conserved in each momentum cell. The edges of continuity cells are called junctions and are at the centers of the momentum cells. The edges of the momentum cells are at the centers of the continuity cells. Discrete values of densities, pressures, and energies are located at the centers of the continuity cells, and discrete values of velocities are located at the centers of the momentum cells. In what follows, continuity cells have the index k and momentum cells have the index j. As you may have noticed earlier, bubbles have the index l. By adopting this convention, the nomenclature is more consistent and easier to understand. In the finite difference equations, variables are needed at locations where they are not defined. Averaging and/or donoring techniques are used to compute these values.

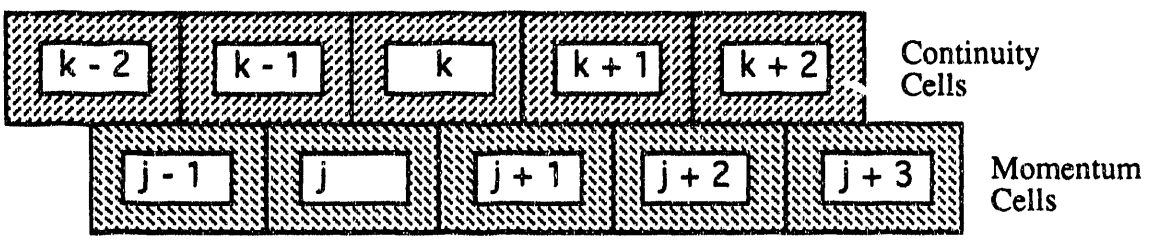

Fig. 1. Continuity and Momentum Cell Locations for the Staggered Eulerian Grid.

3.1. Continuous Phase Mass Equation

The continuous phase mass balance for volume, V_k, is,

$$\frac{d(\alpha_{kl}\rho_{kl}V_k)}{dt} + \left(A_k\alpha_{kl}\rho_{kl}u_{kl}^{n+1}\right)_{in}^{out} = \sum_{l}^{\substack{bubbles\\ in\ cell\ k}}\left\{\eta_{klb}\Gamma_{lbl}^{n+1}\right\} \qquad (7)$$

The average continuous phase velocity at junction j is u_j. The variable, η_{klb}, is defined in the Volume Fraction Coupling section in terms of the bubble volume, V_{lb}, and bubble location, x_{lb}. In equation (7), the second term on the left -hand side represents the net flux of mass out of cell k. As in the particle equations, the time derivatives are expanded, and first-order forward time differences are used with the coefficients evaluated at the old time level.

To prevent a convective instability due to centered mass flux terms, the fluxed densities in equation (7) are donored if the velocity is not zero. Because the bubbles are tracked in a Lagrangian manner, there are no

instabilities associated with α, and the fluxed volume fractions are not donored.

3.2. Continuous Phase Momentum Equation

The continuous phase momentum equation is,

$$\alpha_{jl}\rho_{jl}V_j\frac{du_{jl}}{dt}+\alpha_{jl}\rho_{jl}V_j u_{jl}\left[\frac{u_{jl}-u_{j-1,l}}{\Delta x}\right]= \\ -\alpha_{jl}V_j\left[\frac{P_k^{n+1}-P_{k-1}^{n+1}}{\Delta x}\right]-f_{jwl}u_{jl}^{n+1}-F_{jbl}+\alpha_{jl}\rho_{jl}V_j g \tag{8}$$

The bubble-liquid interphase force, F_{jbl}, is defined as,

$$F_{jbl}=\sum_{\substack{bubbles\\ in\ cell\ j\\ l}}\eta_{jlb}\begin{bmatrix}-f_{lbl}\left(u_{lb}^{n+1}-\{\bar{u}_l\}lb\right)-V_{lb}\left[\frac{\partial P}{\partial x}\right]_{lb}\\ -C_{al}\{\bar{\rho}_l\}_{lb}V_{lb}\left(\frac{du_{lb}}{dt}-\{\bar{a}_l\}_{lb}\right)\end{bmatrix} \tag{9}$$

Consistency between the bubble and the continuous phase momentum interface terms, F_{lb}, given in equation (3) must be satisfied.

The continuity cell variables with a j subscript are simple averages of neighboring continuity cell values. The convective acceleration terms are evaluated using a one-sided upwind spatial gradient (i.e., donoring to make the convective terms stable). In order to make this scheme implicit in the terms responsible for sound wave propagation, the pressure gradient in the momentum equation and the velocity in the mass equation are both evaluated at new time . Hence, this scheme does not have a time step limit based on the sound speed that explicit schemes have.

3.3. Continuous Phase Energy Equation

The conservation of liquid phase energy in cell k is given by the following equation, which is written in terms of entropy, ε_{kl}:

$$\frac{\partial\left(\alpha_{kl}\rho_{kl}\varepsilon_{kl}V_k\right)}{\partial t}+\left(A_k\alpha_{kl}\rho_{kl}\varepsilon_{kl}u_{kl}^{n+1}\right)_{in}^{out}= \\ \frac{Q_{wkl}^{n+1}A_{wk}}{T_{wk}}+\sum_{\substack{bubbles\\ in\ cell\ k\\ l}}\left\{\eta_{klb}\Gamma_{lbl}^{n+1}\varepsilon_{kl}\right\} \\ +\sum\left\{\eta_{klb}\frac{h_{lb}A_{lbl}\left(\theta_{lbl}^{n+1}-\left[w_{lb}T_{kl}^{n+1}+(1-w_{lb})T_{wk}^{n+1}\right]\right)}{\theta_{lbl}}\right\} \tag{10}$$

The weighting factor, w_{lb}, allows us to use a linear combination of the wall temperature and the average liquid temperature. When w_{lb} is one, the bubble sees the average liquid temperature for its heat transfer, and when w_{lb} is zero, the bubble sees the wall temperature for its heat transfer. This

allows us to model subcooled boiling where some bubbles are on the wall and some bubbles are in the free stream.

The second term is the net liquid entropy flux out of cell k through its junctions. The first term on the right-hand-side is the direct entropy addition rate to the continuous liquid phase from the wall heat transfer. Since this energy conservation equation is written in terms of entropy, the wall heat added to the liquid is divided by the source temperature, which is the wall temperature.

The two remaining summation terms account for the energy transfer between the continuous liquid phase and the bubbles. This energy transfer can occur from both mass transfer with its associated phase change and heat transfer. The first summation is the entropy transfer rate associated with mass transfer from the bubble-liquid interface to the continuous liquid phase in cell k. The η_{kib} in this equation is the fraction of bubble i in cell k. The second summation is the heat transfer rate from the bubble-liquid interface to the continuous liquid phase in cell k. The h_{ib} in this equation is the heat transfer coefficient on the outside of the bubble.

4. PHASE COUPLING MODELS

The coupling of the discrete Lagrangian and continuous Eulerian phases proved to be the most difficult part of the modeling and numerical algorithm development. This section describes the coupling models under three headings: (4.1) volume fraction coupling, (4.2) momentum transfer coupling, and (4.3) energy transfer coupling.

4.1. Volume Fraction Coupling

In two-phase bubbly flow, the dispersed phase bubbles can become quite large due to coalescence, merging to form extended cylindrical bubbles that have transverse diameters approaching the pipe diameter. For this reason, the volume occupied by the dispersed particles can not be neglected as it frequently is in modeling liquid sprays [Amsden, 1989].

The volume fraction coupling between the dispersed and continuous phases must be treated carefully. The volume of a bubble located at x_{ib} is clearly discrete in space. The volume fraction, α, in the continuous phase equations results from these spatially discrete bubble volumes. However, in the continuous phase equations, the volume fraction is a continuous field variable with a spatially smooth distribution, as in classical two-fluid models like RELAP5 [Ransom, 1985] and TRAC-BD1 [Taylor, 1984].

This dual character of the volume fraction means that some smoothing interpolation must be used when the bubble volumes are combined to calculate the continuous phase volume fraction. This has been done in DISCON2 using an extended bubble shape function. This should not be confused with the actual shape of the bubble, which is described in Section 5.1. The continuous phase model represents the average phase properties over a region of space comparable to the cell length, Δx. Therefore, in order to smooth out this particle induced continuous phase volume

variation, the particle volume is distributed over an arbitrary length. In the present code, this length is set to the Eulerian cell length, Δx. The code has also run successfully with this arbitrary length set to two or three particle diameters. Because the particle locations are Lagrangian, this smoothing does not introduce any artificial diffusion of the volume fraction. It is simply an interpolation of the volume occupied by the discrete particles onto the continuous field volume fraction, which is itself an average value over the cell.

The cross-sectional area occupied by an extended bubble at position x and time t is given by, $A_{ib}(x,t)$. It will be convenient when we extend the bubble's length to partition the cross-sectional area into the product of two terms, the bubble's volume, $V_{ib}(t)$, and the bubble's shape, $\eta_{ib}(x,t)$. Since, the integral of the cross-sectional area occupied by a bubble, $A_{ib}(x,t)$, over its length is equal to the bubble's volume, $V_{ib}(t)$, the integral of the bubble's shape over the same length has to equal unity. We also require that the shape function not change as the bubble propagates down the pipe, i.e., the (x,t) dependence of the shape function is a function of the relative distance from the bubble's current position, x_{ib},

$$\eta_{ib}(x,t) = \eta_{ib}(q_{ib}) = \eta_{ib}[x - x_{ib}(t)] \tag{11}$$

Thus, we can write the bubble's cross-sectional area as,

$$A_{ib}(x,t) = V_{ib}(t)\eta_{ib}[x - x_{ib}(t)] \tag{12}$$

When we integrate η_{ib} with respect to x over cell k, we get the fraction of bubble i located in cell k,

$$\eta_{kib}(t) = \int_{cell\,k}\{\eta[x - x_{ib}(t)]\}dx \tag{13}$$

If all of bubble i is in cell k, η_{kib} is equal to unity.

The integral of bubble's cross-sectional area equation over cell k times the volume of bubble i divided by the volume of cell k gives the bubble volume fraction in cell k,

$$\alpha_{kib}(t) = \left[\frac{V_{ib}(t)}{V_k}\right]\int_{cell\,k}\{\eta[x - x_{ib}(t)]\}dx = \left[\frac{V_{ib}(t)\eta_{kib}(t)}{V_k}\right] \tag{14}$$

In what follows, we will need the change in the bubble volume fraction over a time step. Therefore, we differentiate equation (14) with respect to time and make use of the fact that the time derivative of $x_{ib}(t)$ is just the bubble velocity, $u_{ib}(t)$, and that the derivative of $q = x - x_{ib}$ with respect to x is 1, to obtain,

$$\frac{d\alpha_{kib}(t)}{dt} = \left[\frac{\eta_{kib}(t)}{V_k}\right]\left[\frac{dV_{ib}(t)}{dt}\right] + \left[\frac{V_{ib}(t)}{V_k}\right]\int_{cell\,k}\left\{\frac{d\eta(q_{ib})}{dq}\right\}dx \tag{15}$$

The integral in this equation can be written as the difference of the "out" minus the "in" values of η at the two junctions at either end of cell k. From Fig. 1, we see that cell k is bounded by junction j on the left and $j+1$ on the right.

$$\frac{d\alpha_{kdb}(t)}{dt} = \left[\frac{\eta_{kdb}(t)}{V_k}\right]\left[\frac{dV_{db}(t)}{dt}\right] - u_{db}(t)\left[\frac{V_{db}(t)}{V_k}\right]\left[\eta\{x_{j+1} - x_{db}(t)\} - \eta\{x_j - x_{db}(t)\}\right] \tag{16}$$

Instead of using the point value of η at junction j, we will use an average value, because this will result in more smoothing of the solution as a bubble moves through a cell.

$$\frac{d\alpha_{kdb}(t)}{dt} = \left[\frac{\eta_{kdb}(t)}{V_k}\right]\left[\frac{dV_{kdb}(t)}{dt}\right] - u_{db}(t)\left[\frac{V_{db}(t)}{V_k}\right]\left[\overline{\eta\{x_{j+1} - x_{db}(t)\}} - \overline{\eta\{x_j - x_{db}(t)\}}\right] \tag{17}$$

The average value of η in a junction is the integral of η over the momentum cell enclosing the junction divided by the length of the junction, Δx.

$$\overline{\eta\{x_j - x_{db}(t)\}} = \left[\frac{1}{\Delta x}\right]\int_{junction\ j}\left[\eta\{x - x_{db}(t)\}\right]dx = \left[\frac{\eta_{jdb}(t)}{\Delta x}\right] \tag{18}$$

The bubble volume fraction in a junction cell is defined, as in equation (14), as

$$\alpha_{jdb}(t) = \left[\frac{V_{db}(t)}{V_k}\right]\int_{junction\ j}\left[\eta\{x - x_{db}(t)\}\right]dx = \left[\frac{V_{db}(t)\eta_{jdb}(t)}{V_k}\right] \tag{19}$$

Using equations (18) and (19) for the average value of η, we can re-write equation (16) in terms of the bubble volume fraction in a junction cell as follows,

$$\frac{d\alpha_{kdb}(t)}{dt} = \left[\frac{\eta_{kdb}(t)}{V_k}\right]\left[\frac{dV_{db}(t)}{dt}\right] - u_{db}(t)\left[\frac{\alpha_{j+1,db}(t) - \alpha_{j,db}(t)}{\Delta x}\right] \tag{20}$$

This is the expression used in the DISCON2 code.

4.2. Momentum Transfer Coupling

The momentum coupling between the discrete particles and the continuous phase is due to the interface force acting on the surface of the particles. In equation (8) the momentum transfer due to mass transfer has been neglected. This interface force is modeled in the particle momentum

equation by the three terms $f_{ibl}\left[u_{ib} - \{\bar{u}_l\}_{ib}\right]$, $V_{ib}\,\partial P/\partial x$, and the added mass term.

The first term represents the classical drag force as measured on a particle immersed in a continuous phase. The drag force is formulated in terms of a drag coefficient, C_d based on the equivalent frontal area. This drag coefficient is obtained from the data correlations of Peebles and Garber [Peebles, 1953] and Harmathy [Harmathy, 1960]. Peebles and Garber give the drag coefficient in the laminar and distorted particle regime. They use a four region formula. Harmathy gives an improved formula for the fourth region and adds a fifth formula for the fully turbulent Taylor cap region. The drag coefficients for bubbles that are used in the DISCON2 were summarized in a previous paper [Trapp, 1991].

When using this formulation for a simulation with many bubbles of various sizes, the question arises of what should be used for the continuous phase far field velocity. In the case of a single bubble rising in a uniform fluid, the appropriate continuous phase far field velocity is clear and is easily determined. In the intermediate situations, the appropriate far field reference velocity is not well defined. For cylindrical bubbles that nearly fill the pipe, the appropriate far field reference velocity is the continuous phase velocity far ahead of or far behind the bubble. Neglecting compressibility effects, this is equivalent to using the mean volumetric flux as the far field reference velocity. At the other extreme of a single small bubble rising in a large tank, the far field velocity is clearly the liquid velocity far from the bubble, which in the limit of vanishing small bubble size is equivalent to the mean volumetric flux.

In the intermediate case, where there are many bubbles of various sizes present in the flow, it is necessary to estimate an equivalent far field velocity for use in the drag correlations. Several papers have recently addressed this problem, see Kowe [Kowe, 1988] and Couet [Couet, 1991]. A reasonable model for the interstitial far field velocity that takes into account the added mass of the continuous phase displaced with the particles has been developed in these references. This model is applicable to low gas volume fraction dispersed flows. When the bubble number density becomes small, the analysis becomes inappropriate. In DISCON2, we consider a full range of bubble number densities and bubble sizes including large cylindrical bubbles filling the pipe. We have chosen to use the mean volumetric flux as the far field reference velocity in all situations. This choice simplified the coding and is appropriate in the limiting cases.

Recalling equation (19), one obtains for the volumetric flux at any junction,

$$\bar{u}_j = \alpha_j u_j + \sum_{\substack{i \\ \text{bubbles in cell } j}} \alpha_{jib} u_{ib} = \alpha_j u_j + \sum_{\substack{i \\ \text{bubbles in cell } j}} \eta_{jib} \frac{V_{ib}}{V_j} u_{ib} \qquad (21)$$

The volumetric far field velocity defined in equation (21) is independent of position when the continuous and particle phases are incompressible and there is no mass transfer. In the numerical simulations, it is important to

represent this far field velocity with a spatially smooth function independent of the Lagrangian nature of the particles. The velocity in equation (21) is consistent with the far field velocities used when the correlations were developed and gives the spatially smooth reference velocity needed in the drag force calculation.

The far field velocity defined above is not the whole story. Each particle can also be influenced by the wake of preceding particles. A trailing particle can be "trapped" in the wake of a leading particle. When a trailing particle, say a bubble rising in a liquid, is in the wake of another bubble, it is rising in a flow field that has a velocity more nearly equal to that of the leading bubble. It rises due to buoyancy in this modified flow field. This is the primary mechanism allowing bubbles to approach and coalesce. This effect is modeled by modifying the far field velocity in equation (21) by the wake velocity of leading particles when making the drag calculation.

The velocity in the wake of a solid object has been discussed in several texts, see for example Batchelor [Batchelor, 1967] and Schlichting [Schlichting, 1955]. In general, for turbulent flow, the wake-induced flow at any position x behind an object can be expressed as,

$$u_{wake} = u_w(x)\exp\left(-\left[\frac{r}{r_w(x)}\right]^2\right) \tag{22}$$

where $u_w(x)$ is the centerline wake velocity, and $r_w(x)$ is a scale for the radial distribution of the wake velocity. A standard integral momentum balance gives the following relationship between $u_w(x)$ and $r_w(x)$,

$$\left[\frac{u_w}{u_r}\right]\left[\frac{r_w}{r_p}\right]^2 = \frac{1}{2}C_d \tag{23}$$

where u_r is the velocity of the wake producing object relative to the fluid, and r_p is the equivalent radius of the particle based upon a spherical shape consistent with the calculation of C_d. Using equations (22) and (23), the velocity at any location behind an object caused by its wake can be found if we know $u_w(x)$ or $r_w(x)$. Stuhmiller [Stuhmiller, 1989] has carried out a preliminary correlation of wake centerline velocity data from several sources and gives a formula for $u_w(x)$,

$$\left[\frac{u_w}{u_r}\right] = \left[a_w + b_w\left(\frac{x}{R_b}\right) + \left(\frac{x}{R_b}\right)^2\right]^{-1} \tag{24}$$

where $a_w = 0.20$, $b_w = 0.12$, $c_w = 0.01$, and R_b is the body or actual radius of the particle. Comparisons of the DISCON2 code calculations with the bubble rise data of Crabreee and Bridgwater [Crabtree, 1971]

were better when we increased a_w to 0.45. Therefore, we used a_w = 0.45 in the current calculations with DISCON2. The bubble shapes are discussed in Section 5.1.

To complete the wake model, the wake velocity of every bubble leading the bubble in question is calculated using the above formulas. There are two wake models in the DISCON2 code, one that uses the "maximum" wake and one that uses the "closest" wake. In both cases, the leading bubble wake velocity is used to calculate the modified far field velocity, $\bar{u}_p$ for the trailing bubble. The trailing bubble thus "sees" this modified far field velocity in its drag correlation. It rises in the wake flow field at a rate determined by the balance of its drag and buoyancy forces. This is the primary mechanism by which trailing bubbles overtake leading bubbles.

The second momentum coupling term, $V_{lb}\,\partial P/\partial x$, represents the average pressure force on the particle surface due to the mean pressure gradient in the continuous phase. This is the source of the buoyancy term that arises for a particle at rest in a stagnant fluid under the action of gravity. In the present version of DISCON2, this effective mean pressure gradient in the continuous phase is modeled using the gravity head and inertial acceleration of the far field continuous phase flow,

$$\frac{\partial \bar{P}}{\partial x} = \{\bar{\rho}\}_{lb}\left[g - \left(\frac{\partial \bar{u}}{\partial t} + \bar{u}\frac{\partial \bar{u}}{\partial x}\right)\right] \tag{25}$$

where $\{\bar{\rho}\}_{lb}$ is the continuous phase density at the location of bubble l.

The third momentum coupling term, added mass, is modeled in the conventional manner using an added mass coefficient of 0.5.

4.3. Energy Transfer Coupling

The energy transfer between the discrete particle and continuous phase is due to heat transfer and mass transfer. The sum of the energy entering the interface plus the energy leaving the interface must equal zero. There can be no accumulation of energy in the interface. This condition is expressed by the following equation, where we are using entropy for the energy variable.

$$\begin{aligned} &-\varepsilon_{lb}\Gamma_{lbl}^{n+1} + \frac{h_{lb}A_{lbl}\left(\theta_{lbl}^{n+1} - T_{lb}^{n+1}\right)}{\theta_{lbl}} \\ &+\varepsilon_{lb}\Gamma_{lbl}^{n+1} + \frac{h_{lb}A_{lbl}\left(\theta_{lbl}^{n+1} - \left[w_{lb}T_{lb}^{n+1} + (1-w_{lb})T_{wlb}^{n+1}\right]\right)}{\theta_{lbl}} = 0 \end{aligned} \tag{26}$$

This first term is the entropy addition rate from the inside of the bubble to the bubble-liquid interface as a result of mass transfer. The second term is the entropy addition rate from the inside of the bubble to the bubble-liquid interface as a result of heat transfer. The third term is the entropy addition rate to the interface from the surrounding liquid as a result of mass transfer.

The last term is the entropy addition rate from the surrounding liquid to the interface as a result of heat transfer.

In the above equation, there are three new variables. These define the average liquid entropy, average liquid temperature, and average wall liquid temperature surrounding bubble i in cell k and are defined as follows,

$$\varepsilon_{lib} = \sum_{k}^{\substack{cells\\surrounding\\bubble\,i}} \left[\eta_{kib} \varepsilon_{kl} \right] \tag{27}$$

$$T_{lib} = \sum_{k}^{\substack{cells\\surrounding\\bubble\,i}} \left[\eta_{lib} T_{kl} \right] \tag{28}$$

$$T_{wib} = \sum_{k}^{\substack{cells\\surrounding\\bubble\,i}} \left[\eta_{kib} T_{wk} \right] \tag{29}$$

5. ADDITIONAL MODELS

Additional models are needed for computing the shape of the bubble. The shape is needed to compute bubble coalescence. In addition, models are needed for bubble turbulence and bubble-liquid heat transfer. We need film heat transfer coefficients on the inside and outside of the bubble-liquid interface. All of these additional models are discussed in this section.

5.1. Bubble Shape Model

So far in the development, the actual shape of the dispersed particle has not been a factor in the model. The drag correlations are based upon the frontal area of an equivalent sphere having volume V_p, and the actual shape has not been needed.

In general, bubbles, and to a lesser degree drops, take on a variety of shapes depending upon their size. The sequence of shapes shown in Fig. 2 is generally characterized in increasing volume as sphere, oblate spheroid, Taylor cap, and cylindrical bubble. We used the simple formulas given by Stuhmiller [Stuhmiller, 1989] to characterize each shape. These formulas are based upon the Eötvos number, E, the particle volume, V_p, and the pipe radius, R.

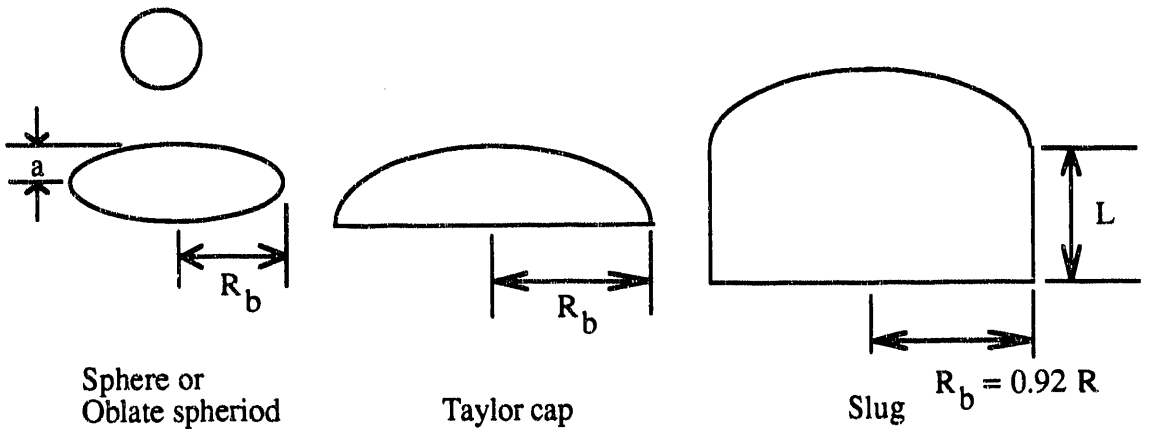

Fig. 2. Calculated Bubble Shapes.

The Eötvos number is defined as follows,

$$E = 4gr_p^2\left[\frac{|\rho - \rho_p|}{\sigma}\right] \tag{30}$$

These shapes are explicitly used at two places in the model and in all visual output from a DISCON2 simulation. The body or actual radius of the particle, R_b, is used in the wake centerline velocity calculation, equation (24). Both the particle radius, R_b, and the actual vertical height of a particle are used in the bubble coalescence model.

5.2. Bubble Coalescence Model

Two bubbles merge or coalesce if they overlap in the radial and axial directions by more than a certain fraction, called the overlap fraction. The bubble shapes are used in the computation of this overlap fraction. The overlap fraction is an input parameter, and in most simulations, it is set to zero, i.e., the two bubbles merge when they just touch. When two bubbles are merged, the sum of their masses, momenta, and entropies are preserved. The merged bubble is placed at the center of mass of the two original bubbles. Only bubbles that are in the free stream are merged. All the bubbles on the wall retain their identity even if they overlap another bubble. They can only merge after they are released from the wall.

Future extensions of the merging criterion will include the addition of a delay time to account for time it takes the liquid film between the bubbles to drain away. This phenomena has been observed experimentally.

5.3. Bubble Turbulence Model

A very simple turbulence model is used to simulate the effect of the fluctuating continuous phase velocity field. The velocity of each particle is assumed to consist of the deterministic velocity component plus an additive fluctuating component generated by the turbulence present in the continuous phase. The particle positions are then calculated using the following equations,

$$\frac{dx_{lb}}{dt} = u_{lb}^{n+1} + u'_{lb} \tag{31}$$

$$\frac{dy_{lb}}{dt} = v'_{lb} \tag{32}$$

$$\frac{dz_{lb}}{dt} = w'_{lb} \tag{33}$$

where u'_{lb}, u'_{lb}, and w'_{lb} are the velocities generated by the continuous phase turbulence in the x, y, and z directions respectively. These fluctuating continuous phase velocities are related to the intensity of the turbulent wakes produced by the neighboring particles (wall effects are neglected). A simple random walk process that produces the same fluid parcel dispersion as found in homogeneous turbulence as developed by Tennekes and Lumley [Tennekes, 1972] is used to estimate the size of u'_{lb}, u'_{lb}, and w'_{lb}, see Stuhmiller [Stuhmiller, 1989].

5.4. Wall Heat Transfer Model

A wall heat transfer model has been developed for forced convection, subcooled boiling, and saturated boiling. The forced convection and saturated boiling models are conventional, but the subcooled boiling model is unique and will be explained in more detail.

In subcooled boiling, the average liquid temperature is less than the saturation temperature, so in theory, no boiling can take place. However, if the heat flux is large enough, the wall temperature will be higher than the saturation temperature, the fluid adjacent to the wall will be above the saturation temperature, and subcooled boiling can take place. The subcooled boiling model partitions the heat flux into two parts: that driven by the difference in the wall temperature and the bulk liquid temperature, and that driven by the difference in the wall temperature and the liquid saturation temperature. In the subcooled boiling model, a portion of the heat goes into heating up the liquid phase, and the remainder goes into creating and growing bubbles that are attached to the wall. Once the bubbles get large enough, they are released into the bulk liquid phase where they can either grow or condense.

For the wall heat flux to the liquid, we have,

$$Q_{wkl}^{n+1} = h_{kl,mic}\left[T_{wk}^{n+1} - \hat{T}_{sat}\left(P_k^{n+1}\right)\right] + h_{kl,mac}\left[T_{wk}^{n+1} - T_{kl}^{n+1}\right] \tag{34}$$

where the heat transfer coefficients are taken from the Chen [Chen, 1966] correlation. This equation is used in DISCON2 to determine the wall temperature. The wall heat flux to the liquid is an input quantity.

5.5. Bubble-Liquid Heat Transfer Model

The bubble–liquid heat transfer model consists of two models: one for the inside of the bubble and one for the outside of the bubble. The outside heat

transfer model is further modified when the bubble is on the wall at a boiling nucleation site.

Inside the bubble, we use a relaxation model to compute the heat transfer coefficient,

$$H_{ib} \equiv \left[\frac{h_{ib}A_{ibi}}{\theta_{ibi}}\right] = \left[\frac{V_{ib}\rho_{ib}}{\tau_{hb}}\right]\left[\frac{d\varepsilon_{ib}}{dT}\right] \tag{35}$$

where τ_{hb} is the relaxation time constant for the bubble temperature. The relaxation time constant is the time it takes the bubble temperature to come within about 63% of its final value after a step change in the bubble-liquid interface temperature. After about 5 time constants, the bubble temperature is within 99% of the interface temperature. This relaxation time constant is input and in most calculations it is usually set to 20% of the time step to assure that the bubble temperature stays close to the saturation temperature at each time step.

Outside the bubble, when it is in the free stream, i.e., not attached to a wall nucleation site, we use a heat transfer model from Whitaker [Whitaker, 1972] for heat transfer to a sphere in a flowing fluid.

$$H_{ib} \equiv \left[\frac{h_{ib}A_{ibi}}{\theta_{ibi}}\right] = \left[\frac{A_{ibi}}{\theta_{ibi}}\right]\left[\frac{k_l}{2R_{eq_{ib}}}\right]\left[2 + \left(0.4\,\mathrm{Re}_{ib}^{0.5} + 0.06\,\mathrm{Re}_{ib}^{0.67}\right)\mathrm{Pr}_{ib}^{0.4}\right] \tag{36}$$

where the Reynolds number is defined as

$$\mathrm{Re}_{ib} = \left|u_{ib} - \{\bar{u}_l\}_{ib}\right|\left[\frac{2R_{eq_{ib}}}{\nu_l}\right] \tag{37}$$

and the Prandl number is defined as

$$\mathrm{Pr}_{ib} = \frac{\{\bar{C}_{p_l}\}_{ib}\,\nu_l\{\bar{\rho}_l\}_{ib}}{k_l} \tag{38}$$

When the bubble is attached to a wall nucleation site, we compute an equivalent heat transfer coefficient from a combination of Lahey's model [Lahey, 1978] for subcooled boiling, Saha and Zuber's correlation [Saha, 1974] for the critical enthalpy for net generation of vapor, and the Chen correlation [Chen, 1966]. This combination of models is also used in the TRAC-BD1 computer code [Taylor, 1984].

The partitioning of the heat transferred from the wall into the growing of bubbles and heating of liquid is taken from Lahey's model [Lahey, 1978] for subcooled boiling. The mass transfer rate from the wall to the bubbles on the wall is given by

$$\Gamma_{wkb} = \frac{Q_{wkl}A_{wk}M_{kl}}{\left[\hat{i}_{g,sat}(P_k) - i_{kl}\right]} \tag{39}$$

where M_{kl} is a multiplier that gives the fraction of the wall heat flux that goes to making bubbles. It is given by,

$$M_{kl} = \frac{i_{kl} - i_{kl,cr}}{\left[\hat{i}_{l,sat}(P_k) - i_{kl,cr}\right]\left[1 + \psi_{kl}\right]} \tag{40}$$

where ψ_{kl} is given by,

$$\psi_{kl} = \frac{\rho_{kl}\left[\hat{i}_{l,sat}(P_k) - i_{kl}\right]}{\hat{\rho}_{g,sat}(P_k)\left[\hat{i}_{g,sat}(P_k) - \hat{i}_{l,sat}(P_k)\right]} \tag{41}$$

In equations (40) and (41), the critical enthalpy is the enthalpy the fluid to exceed before there is a net generation of vapor. It is given by the Saha-Zuber model [Saha, 1974] as,

$$h_{kl,cr} = \left\{ \begin{array}{l} \hat{i}_{l,sat}(P_k) - \dfrac{St_{kl} C_{p_l}}{0.0065} \text{ for } Pe_{kl} > 70,000 \\ \hat{i}_{l,sat}(P_k) - \dfrac{Nu_{kl}^{'} C_{p_l}}{445} \text{ for } Pe_{kl} \le 70,000 \end{array} \right\} \tag{42}$$

The Stanton number is defined as,

$$St_{kl} = \frac{Nu_{kl}^{'}}{Pe_{kl}} \tag{43}$$

and the modified Nusslet number, which is the Nusslet number times the temperature difference, is defined as,

$$Nu_{kl}^{'} = \frac{Q_{wk} D_{e_{kl}}}{k_l} \tag{44}$$

The Pecklet number is defined as,

$$Pe_{kl} = \frac{G_{kl} D_{e_{kl}} C_{p_l}}{k_l} \tag{45}$$

This set of equations determines the mass transfer rate from the fluid on the wall into bubbles attached to the wall nucleation sites. If we now modify the heat transfer coefficient on the liquid side of the bubbles on the wall as given by the Chen correlation for $h_{kl,mic}$ we can let the code compute the correct amount of mass to transfer from the liquid phase to the bubbles on the wall. In this case, the conservation of energy at the bubble-liquid interface, equation (26), can be simplified to

$$(\varepsilon_{tb} - \varepsilon_{tlb})\Gamma_{tbl} = H_{tlb}(\theta_{tlb} - T_{wtb}) \tag{46}$$

where we have set $w_{tlb} = 0$ because the bubble is on the wall and $T_{tb} = \theta_{tbl}$ because the bubble is small and its internal temperature cannot differ very

much from its interface temperature. We have also combined three terms, $h_{lib}A_{ibl}/\theta_{ibl}$, into H_{lib}.

We substitute into equation (46) the relationship obtained above for the bubble–liquid mass transfer rate and get,

$$\frac{Q_{wkl}A_{wk}M_{kl}(\varepsilon_{ib}-\varepsilon_{lib})}{N_{kl}\left[\hat{i}_{l,sat}(P_k)-i_{kl}\right]}=H_{lib}(\theta_{ibl}-T_{wib}) \tag{47}$$

where N_{kl} is the number of bubbles on the wall in cell k. Notice, that by dividing by N_{kl} we have assumed that all the bubbles on the wall have equal rights and get an equal share of the wall heat flux. Another option would be to partition the heat flux according to the size of the bubble.

Substituting for the wall heat flux to the liquid from the Chen correlation, and noting that the saturation temperature in this equation, T_{sat}, is the same as the interface temperature, θ_{ibl}, and for small bubbles, the temperature of the liquid surrounding a bubble, T_{wil}, is close to the wall temperature, T_{wk}, we can write the equation (47) as,

$$\left\{\frac{F_{wkl}A_{wk}M_{kl}(\varepsilon_{ib}-\varepsilon_{lib})}{N_{kl}\left[\hat{i}_{l,sat}(P_k)-i_{kl}\right]}\right\}\left\{h_{kl,mic}\left[T_{wk}-\theta_{ibl}\right]+h_{kl,mac}\left[T_{wk}-T_{kl}\right]\right\} \tag{48}$$
$$=H_{lib}(\theta_{ibl}-T_{wk})$$

Solving equation (48) for H_{lib}, we get,

$$H_{lib}\equiv\frac{h_{lib}A_{ibl}}{\theta_{ibl}}=-\left\{\frac{F_{wkl}A_{wk}M_{kl}(\varepsilon_{ib}-\varepsilon_{lib})}{N_{kl}\left[\hat{i}_{l,sat}(P_k)-i_{kl}\right]}\right\}\left\{h_{kl,mic}+h_{kl,mac}\left[\frac{T_{wk}-T_{kl}}{T_{wk}-\theta_{ibl}}\right]\right\} \tag{49}$$

When we use this value for H_{lib}, bubbles attached to wall nucleation sites will grow to create the same void fraction as would be produced in more conventional two-phase codes like RELAP5 [Ransom, 1985] and TRAC-BD1 [Taylor, 1984] when they use the Lahey, Saha-Zuber, and Chen models.

While this subcooled boiling model for H_{lib} is somewhat unconventional, it is used here because we have not found any appropriate correlations for the heat transfer coefficient on the outside of bubbles attached to wall nucleation sites. However, the DISCON2 code is certainly capable of using such correlations if and when they become available.

6. SUMMARY OF BASIC EQUATIONS

For the discrete phase, the basic equations are the mass conservation (1), the momentum balance (2), energy balance (5), and the kinematic position equation (6). The continuous field equations for each cell are the mass conservation (7), the momentum balance (8), and the energy conservation

(10). In addition, there is the energy transfer coupling (26). The above seven equations (per particle, per cell) are the basic equations to be solved for the seven new time variables, $V_{lb}, u_{lb}, \varepsilon_{lb}, x_{lb}, P_k, u_j, and\ \varepsilon_k$. The formulas of Section 4.1, are used to express the volume fraction, α_k, in terms of the particle volume, V_{lb}. The remaining new time values of the state variables, ρ_{lb} and ρ_k, are functions of the independent state variables, P_k and T_k. The present version of DISCON2 neglects any pressure difference between the phases; therefore, P_k (when interpolated to a particle position) forms an independent state variable for the particle phase. All state relationships in DISCON2 are linearized during a time step.

An examination of the basic finite difference equations reveals the following:

- They are linear in the new time variables. Hence, each time advancement only requires the solution of a linear system of equations. This is a very complicated linear system due to the mixed Lagrangian and Eulerian features of the equations and the implicit coupling between the phases caused by the time derivatives of α_k in equations (7) and (10).
- The acoustic terms (i.e., velocities in equation (7) and pressure gradient in equation (8)) are evaluated implicitly, hence there is no upper limit on the allowable time step size due to acoustic wave propagation.
- The drag term in the particle momentum equation is evaluated implicitly in u_{lb}. Hence, the short time constant associated with the large drag force on the particle does not lead to a stability restriction on the time step size.

Because of the explicit evaluation of the convective terms in the continuous phase, the time step size is restricted by the material Courant limit . In addition to the material Courant limit stability restriction on Δt, the step size must be chosen to resolve the accuracy of the important physics of any given process.

7. SOLUTION SCHEME

The solution scheme is a semi-implicit scheme and is outlined below for one time step of the calculation.

At the beginning of each time step, the volumetric flux and average acceleration is computed from continuous phase velocities and particle velocities. Next, any particles that satisfy the coalescence criteria are merged. If two particles overlap by some specified fraction, which is input, the two particles are replaced by one particle having a mass equal to the sum of the masses of two merged particles, a momentum equal to the sum of

the momenta of the two merged particles, an entropy equal to the sum of the entropies of the two merged particles, and volume equal to the sum of the volume of the two merged particles. The new particle is located at the center of mass of the two merged particles. The pressure of the new particle is a mass weighted average of the pressure of the two merged particles.

The shape of the particle is then computed, and the heat transfer coefficients are computed from correlations. The drag coefficient is determined using correlations discussed in Section 4.2. The wake velocities at each particle's position due to each of the leading particles is computed using the other equations in Section 4.2. Terms that go into the discrete phase momentum equation are now known, and the new time particle velocity is computed using equation (2). The new time particle position is then computed from equation (6).

The integrated effects of the particles on the continuous phase are computed. These effects are contained in the last term of equation (8), which is a summation over all the particles in a momentum control volume. The continuous phase velocity for each momentum cell is computed using equation (8). Since we do not know the new time pressure gradient yet, this velocity is explicit and uses the old time pressure gradient, $P_k^n - P_{k-1}^n$. We also compute an influence coefficient, $vdp_j = -\Delta t/(\rho_j \Delta x)$, that can later be multiplied by the gradient of the new time pressure increment, $\Delta P_k^{n+1} - \Delta P_{k-1}^{n+1}$, and added to the explicit velocity, u_j^{exp}, to obtain the new time velocity,

$$u_j^{n+1} = u_j^{exp} + vdp_j\left[\Delta P_k^{n+1} - \Delta P_{k-1}^{n+1}\right] \tag{50}$$

The new time pressure increment, $\Delta P^{n+1} = P^{n+1} - P^n$, is computed using an expanded form of the continuous phase mass equation, equation (7),

$$\rho_k V_k \frac{\partial \alpha_k}{\partial t} + \alpha_k V_k \left[\frac{\partial \rho_k}{\partial P}\right]\frac{\partial P_k}{\partial t} + A\left(\alpha_{j+1}\rho_{j+1}u_{j+1}^{n+1} - \alpha_j \rho_j u_j^{n+1}\right) = \sum_{\substack{t \\ \text{bubbles} \\ \text{in cell } k}} \left\{\eta_{kib}\Gamma_{ibl}^{n+1}\right\} \tag{51}$$

where we have expanded the time derivative into two terms. We replace the two velocities in the mass flux term in this equation with a suitable form of equation (50). For the derivative of the volume fraction, $\partial \alpha_k / \partial t$, we use equation (20), which brings in a dV_{ib}/dt term, which can be expressed using an expanded form of the bubble phase mass equation, equation (1),

$$\rho_{ib}\frac{dV_{ib}}{dt} + V_{ib}\frac{d\rho_{ib}}{dP}\frac{dP}{dt} = -\Gamma_{ibl}^{n+1} \tag{52}$$

We do a similar expansion on the bubble energy equation, equation (5),

$$\rho_{lb}\varepsilon_{lb}\Delta V_{lb} + V_{lb}\left\{\left[\frac{\partial(\rho_{lb}\varepsilon_{lb})}{\partial P}\right]\Delta P_{lb} + \left[\frac{\partial(\rho_{lb}\varepsilon_{lb})}{\partial T}\right]\Delta T_{lb}\right\} \tag{53}$$
$$+\varepsilon_{lb}\Delta t\Gamma_{lbl}^{n+1} - H_{lb}\Delta t(\Delta\theta_{lbl} - \Delta T_{lb}) = H_{lb}\Delta t(\theta_{lbl} - T_{lb})$$

Thus, equations (52) and (53) become a block tridiagonal system of equations involving only the pressure and temperature increments in cell *k*, and the pressure increment in its adjacent neighboring cells, *k+1* and *k-1*. This tridiagonal system is solved for the pressure and temperature increments in each cell using a Gaussian elimination solver.

With the new time pressure and temperature increments are known, the new time continuous phase velocity is computed using equation (50), and the new time particle volume is computed using equation (52).

The continuous phase and the particle phase densities are computed from an appropriate state equation. Using the new time particle volume, the fraction of each particle in cell *k*, η_{klb}, and junction *j*, η_{jlb}, is computed using equations (14), and (19). The volume fractions of the continuous phase in each cell and junction are also computed at this time.

This concludes one time step of the calculation, and we repeat these steps for the next time step.

8. TEST PROBLEMS

This section documents several DISCON2 simulations of experiments performed by Carl St. Pierre [St, 1965,St, 1967]. While there may be more recent data, this data was used because it was the same data that was used by Stuhmiller to test out his BUBBLE code [Stuhmiller, 1989].

Each simulation can viewed as a another numerical experiment. Repeating a run will gives different results because of the randomness in the locations of the bubble nucleation sites and bubble turbulence.

8.1. St. Pierre Experiment

Two runs were simulated, Run 1 and Run 10. Run 1 had the lowest pressure, 200 psia (1.38 MPa), and the lowest inlet subcooling, 0.5 F (0.28K). Run 10 a higher pressure, 600 psia (4.14 MPa), and the highest inlet subcooling, 12.6 F (7.00K). Both runs had an inlet velocity of 3.78 ft/s (1.152 m/s). The wall heat flux in Run 1 was 2.28 Btu/hr-ft^2 (7.19x10^4 W/m^2) and in Run 10 it was 9.12 Btu/hr-ft2 (2.88x10^5 W/m^2).

The channel was rectangular and had dimensions of 0.437x1.750 in. (1.11x4.445 cm). The heated length was 49.5 in. (125.7 cm), and the total length was 61 in. (154.9 cm). A power supply that could output 100 V at 3000 A supplied the heating. The void fraction measurements used the gamma-ray attenuation technique. St. Pierre estimated the error in the average void fraction at less than 10%. Measurements were made at thirteen equidistant locations along the channel, and in all cases, the gamma-ray beam passed through the 1.75-in. depth of the channel. Traversal of the channel in the narrow direction provided void fraction

measurements across the channel. These were averaged to get the average void fraction data at one of ten axial locations. Due to small misalignments, only 80% of the cross section could be traversed. St. Pierre states that this limitation would tend to give higher void fractions for the downstream portion of the test section where convex void fraction distributions were present and lower fractions near the inlet where concave distributions were present.

We modeled the experiment with 10 cells in the heated section with 2 cells on either end for a total of 14 cells. Time steps of 5 ms were used. The water was initialized with a uniform pressure and temperature. The wall heat flux activated at cycle 5 after the gravity head in the water had built up. We used the "maximum" model for bubble coalescence. Most of the runs were 500 cycles long and from the results, steady state was reached by 300 cycles. Bubbles were released from the wall when their radius exceeded 1 mm. Their initial radius was 0.001 mm. The turbulence parameter was set to zero, i.e., there was no turbulence model for these runs. The runs were made with 10 active nucleation sites on the wall. The nucleation sites were randomly picked.

8.2. St. Pierre Run 10 Comparisons

Run 10 had an inlet subcooling of 7.0 K. Fig. 3 shows a comparison of the DISCON2 calculation with the experimental data. We put ±10% error bars on the experimental data, as recommended by St. Pierre. The data for the calculation are averaged over 100 cycles, from cycle 400 to 500. The experimental data is above the calculation is good over most of the range. The calculated void has a general tendency to be under the experimental data in the upper end of the channel.

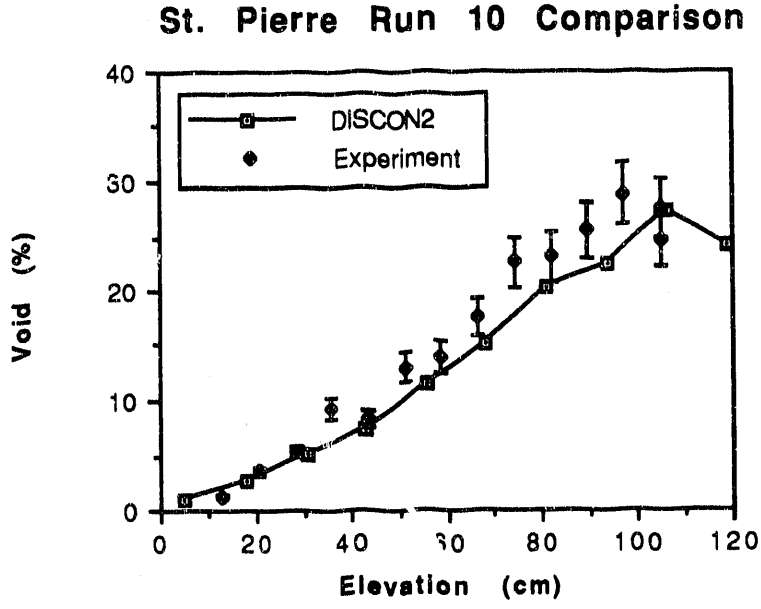

Fig. 3. Comparison of Averaged Void Fraction for St. Pierre Run 10 and DISCON2 Calculation.

Fig. 4 shows the total number of bubbles at each cycle in the simulation of Run 10. Since we activated 10 nucleation sites in each of the 10 cells, 100 of these bubbles were on the wall at nucleation sites. That leaves about 1000 bubbles in the free stream after the initial transient has dissipated (after cycle 100) None of the bubbles released from the wall collapsed in the free stream. Evidently, they all coalesced with existing bubbles in the free stream before they had time to collapse. The fluctuation in the number of bubbles gives an indication of the statistical nature of the calculation. A repeat of this calculation with a different set of wall nucleation sites could easily result in a different number of bubbles at each cycle.

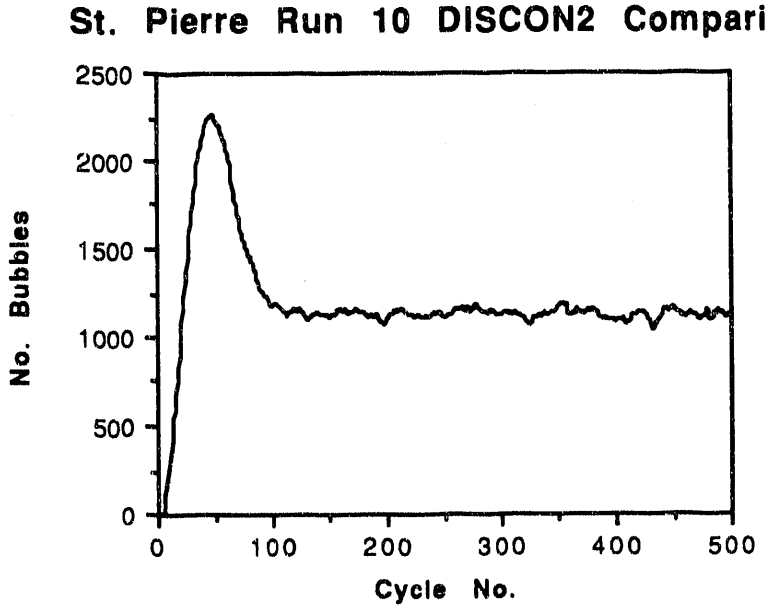

Fig. 4. Total Number of Bubbles in the Channel for the DISCON2 Simulation of the St. Pierre Experiment Run 10.

Fig. 5 shows the liquid, wall, and saturation temperatures for the DISCON2 simulation of Run 10. Since the wall heat flux is constant and the wall temperature is almost parallel with to the saturation temperature, we see that the h_{mic} portion of the Chen correlation is the dominating term in the wall temperature model. There is some slight curvature of the wall temperature at the entrance, which indicates that if the subcooling was larger, the h_{mac} portion of the Chen correlation would come into play and the wall temperature would parallel the liquid temperature. (See Fig. 5.1 in Collier [Collier, 1972]).

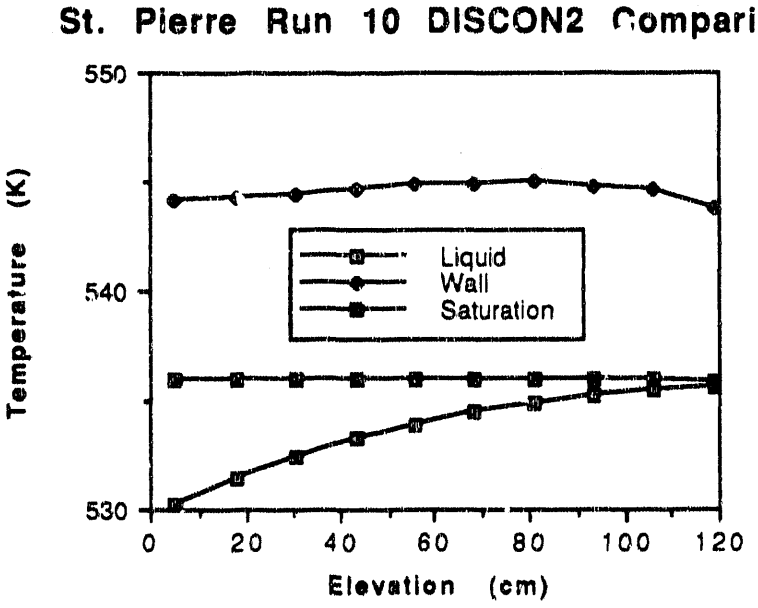

Fig. 5. Liquid, Saturation, and Wall Temperatures for the DISCON2 Simulation at Cycle 500 of the St. Pierre Experiment Run 10.

8.3. St. Pierre Run 1 Comparisons

Run 1 had an inlet subcooling of 0.28 K. Fig. 6 shows a comparison of the DISCON2 calculation with the experimental data. We again put ±10% error bars on the experimental data. The DISCON2 data shown are averaged over 100 cycles, from cycle 400 to 500. The agreement of the calculation with the experiment is good over most the channel length. There is some under prediction of the experimental data around 40 cm and again at 100 cm.

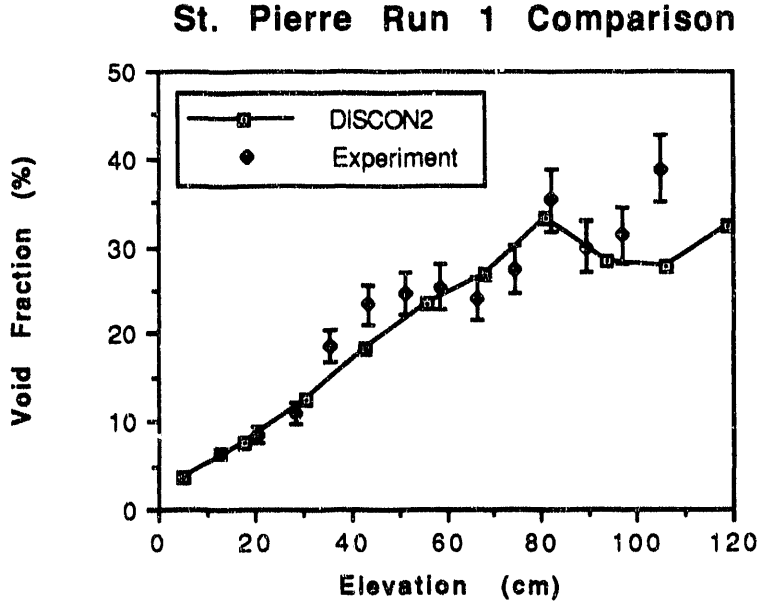

Fig. 6. Comparison of Averaged Void Fraction for St. Pierre Run 1 and DISCON2 Calculation.

9. CONCLUSIONS

The discrete particle two-phase flow model is able to dynamically predict the evolution of both the flow topology and energy partitioning as the bubbles form on the wall and merge due to wake effects. Many more simulations are required, however, including larger subcooling experiments and the transition from long Taylor bubbles to annular flow. Our goal is to be able to simulate a boiling experiment that has subcooled water at the entrance and superheated steam at the exit. However, before this simulation can be done, we need to add the continuous gas phase with its discrete drops. We also need to improve the heat transfer models for bubbles attached to wall nucleation sites. Work along these lines is in progress and will be reported in due course.

10. REFERENCES

Amsden, A.A., O'Rourke, P.J., and Butler, T.D., KIVA-II: A Computer Program for Chemical Reactive Flows with Sprays, Technical Reptort LA-11560-MS, Los Alamos National Laboratory, Los Alamos, NM, May, 1989.

Batchelor, G.K., *An Introduction to Fluid Dynamics*, Cambridge at the University Press, London, 1967.

Chen, J.C., "Correlation for Boiling Heat Transfer to Saturated Fluids in convective Flow," *I & E C Process Design and Development*, Vol. 5, pp. 322–329 (July, 1966).

Collier, J.G., *Convective Boiling and Condensation*, McGraw-Hill, 1972.

Couet, B., Brown, P., and Hunt, A., "Two-Phase Bubbly-Droplet Flow through a Contraction: Experiments and a Unified Model," *Int. J. Multiphase Flow*, Vol. 17, pp. 291–307 (1991).

Crabtree, J.R. and Bridgwater, J., "Bubble Coalescence in Viscous Liquids," *Chem. Engr. Sci.*, Vol. 26, pp. 839–851 (1971).

Dukowicz, J.K., Quasi-Steady Droplet Phase Change in the Presence of Convection, Technical Reptort LA-7997-MS, Los Alamos National Laboratory, Los Alamos, NM, August, 1979.

Harmathy, T.Z., "Velocity of Large Drops and Bubbles in Media of Infinite or Restricted Extent," *AIChE J.*, Vol. 6, pp. 281–288 (1960).

Kowe, R., Hunt, J.C.R., Hunt, A., Couet, B., and Bradbury, L.J.S., "The Effects of Bubbles on the Volume Fluxes and the Pressure Gradients in Unsteady and Non-Uniform Flow of Liquids," *Int. J. Multiphase Flow*, Vol. 14, pp. 587–606 (1988).

Lahey, R.T., "A Mechanistic Subcooled Boiling Model," In *Proceedings of the Sixth International Heat Transfer Conference in Toronto, Canada*, ASME, 1978, pp. 293–295.

O'Rourke, P.J., *Collective Drop Effects in Vaporizing Liquid Sprays*, Ph.D. Thesis, Ph. D. Thesis 1532-T, Princeton University, Princeton, NJ, November 1981.

O'Rourke, P.J. and Amsden, A.A., "The Tab Method for Numerical Calculation of Spray Droplet Breakup," In *International Fuels and Lubricants Meeting and Exposition, Toronto, Ontario*, Society of Automotive Engineers, November, 1987.

Peebles, F.N. and Garber, H.J., "Studies in the Motion of Gas Bubbles in Liquids," *Chem. Engr. Progress*, Vol. 49, pp. 88–97 (1953).

Ransom, V.H., RELAP5/MOD2 Code Manual, Technical Reptort NUREG/CR-4312 and EGG-2396, EG&G Idaho, August, 1985.

Saha, P. and Zuber, N., "Point of Net Vapor Generation and Vapor Void Fraction in Subcooled Boiling," In *Proceedings of the 5th International Heat Transfer Conference, Tokyo*, ASME, 1974.

Schlichting, H., *Boundary Layer Theory*, Pergamon Press, New York, 1955.

St. Pierre, C.C., *Frequency Response Analysis of Steam Voids to Sinusoidal Power Modulation in a Thin Walled Boiling Water Coolant Channel*, Ph.D. Thesis, Northwestern University, 1965.

St. Pierre, C.C. and Bankoff, S.G., "Vapor volume Profiles in Developing Two-Phase Flow," *Int. J. Heat Mass Transfer*, Vol. 10, pp. 237–249 (1967).

Stuhmiller, J.H., Ferguson, R.E., and Meister, C.A., Numerical Simulation of Bubbly Flow, Technical Reptort EPRI NP-6557, Electric Power Research Institute, Palo Alto, CA, November, 1989.

Taylor, D.D., TRAC-BD1/MOD1: An Advanced Best Estimate Computer Program for Boiling Water Reactor Transient Analysis, Technical Reptort NUREG/CR-3633 and EGG-2294, EG&G Idaho, April, 1984.

Tennekes, H. and Lumley, J.L., *A First Course in Turbulence*, MIT Press, 1972.

Trapp, J.A., Mortensen, G.A., and Ransom, V.H., "Particle-Fluid Two-Phase Flow Modeling," In *Advances in Mathematics, Computations, and Reactor Physics*, American Nuclear Society, April, 1991.

Whitaker, S., "Forced Convection Heat-Transfer Correlations for Flow in Pipes, Past Flat Plates, Single Cylinders, Single Spheres, and Flow in Packed Beds and Tube Bundles," *AIChE J.*, Vol. 18, pp. 361 (1972).

END

DATE
FILMED
10/6/92